Engineering Optimization
Vol. 41, No. 5, May 2009, 419–435

Taylor & Francis
Taylor & Francis Group

State-transition-matrix optimization for reconfiguration manoeuvres of formation-flying satellites

Jesse Eyer* and Christopher Damaren

University of Toronto Institute for Aerospace Studies, 4925 Dufferin Street, Toronto, Ontario, Canada, M3H 5T6

(*Received 13 February 2008; final version received 15 October 2008*)

The on-orbit reconfiguration of a pair of formation-flying satellites in low Earth orbit is studied in the presence of J_2–J_6 gravitational perturbations. A methodology for determining a robust and accurate impulsive thrusting scheme is developed with the aim of minimizing reconfiguration overshoot errors and fuel expenditure (ΔV). The method uses a state transition matrix based on the Hill–Clohessy–Wiltshire linear equations of relative motion and the analytical solution to the state-space model to solve for a pair of impulsive thrusts. The manoeuvre is then propagated through a fully nonlinear orbital simulator with the thrusts implemented non-impulsively. A Sequential Quadratic Programming optimizer adjusts the inputs to the linear state transition matrix to produce impulses that, when applied in the high-fidelity orbital propagator, mitigates the ΔV of the manoeuvre while maintaining acceptable overshoot errors.

Keywords: formation-flying satellites; overshoot error; reconfiguration optimization; state transition matrix

1. Introduction

One of the advantages of formation-flying satellites is their capability to reconfigure their formations *in situ* to adapt to multiple mission requirements. Methods for reconfiguring the satellites, whether through impulsive open-loop manoeuvres or closed-loop feedback control, must be fuel efficient, accurate, robust, and work effectively in a real orbital environment.

Dimitriu *et al.* (2007) proposed a formation-flying demonstration in which three satellites are stationed in a geostationary transfer orbit. The two controlled deputy satellites must transfer from a random disposition on an 8km sphere to a 250m isosceles triangle configuration with the uncontrolled chief satellite. Although the control solution uses continuous thrusting with closed-loop feedback and reference trajectory designs based on Pontryagin's maximum principle, the method has a very small stability region and the reconfiguration manoeuvre achieves an accuracy of only $\pm$8m.

Lovell and Tragesser (2004) developed a three-thrust impulsive reconfiguration scheme based on solutions to the Hill–Clohessy–Wiltshire (HCW) equations. The scheme provides a simple and

*Corresponding author. Email: eyer@utias.utoronto.ca

ISSN 0305-215X print/ISSN 1029-0273 online

DOI: 10.1080/03052150802582167
http://www.informaworld.com

convenient method for transferring between different along track orbit (ATO) formations, or from ATO formations into projected circular orbit (PCO) formations. Vaddi *et al.* (2005) completed the technique by developing a dual-thrust, impulsive method for transferring between two PCO orbits of different radii. In each case, however, the techniques are based on Keplerian mechanics and are valid only for circular orbits.

State transition matrices (STMs) can be used in conjunction with the analytical solution of a state-space model to develop the impulses required for reconfiguration manoeuvres. Those STMs based on the linear HCW equations, however, are inaccurate on large time scales (*i.e.* one orbital period), and researchers have sought to improve upon them. Gim and Alfriend (2003) used a geometric method to derive an STM for formation-flying satellites in arbitrarily eccentric orbits under the influence of J_2 perturbation. The STM is presented in terms of both mean and osculating orbital elements, but is highly complex and deemed too computationally demanding to be solved in real-time onboard a satellite. These authors later re-examined their STM for minimum energy reconfiguration purposes (Yan and Alfriend 2007). The resulting reconfiguration trajectories are slow, spiral transfers between PCO orbits of differing radii, and require continuous thrusting with feedback control. Researchers have also solved for STMs that function well in a broad range of elliptical orbits (Yamanaka and Ankersen 2002, Lee *et al.* 2007). Although these STMs outperform the HCW equations, they fail to take gravitational perturbations into consideration, which would lead to high overshoot errors in a real orbital environment.

Optimization has been previously employed for the purposes of satellite formation reconfiguration. Mailhe and Guzman (2004) used a combination of a genetic algorithm and Lawden's primer vector theory to find the optimal number of thrusts to minimize the overall ΔV requirements. Boutonnet and Martinot (2005) also used the primer vector theory to analytically optimize fuel consumption during satellite formation deployment. In both cases, however, the authors established optimal reconfiguration manoeuvres in the absence of orbital perturbations, thus limiting their practical application.

In this study, an STM based on the HCW equations is combined with an SQP optimization algorithm to develop accurate and low ΔV reconfiguration manoeuvres for formation-flying satellites. Although this method calculates the reconfiguration impulses using linearized relative dynamics, the optimizer adjusts the inputs to the STM according to the nonlinear orbital equations of motion with J_2–J_6 perturbations. Consequently, the final reconfiguration impulse solutions work well in a realistic orbital environment. This reconfiguration method is applied to a simulation of the CanX-4&5 formation-flying nanosatellite mission currently under development at the University of Toronto. CanX-4&5 are scheduled to demonstrate a 1,000 m ATO formation, a 500 m ATO, a 50 m PCO, and finally a 100 m PCO. The satellites will perform 50 orbits in each formation, and to transition between each formation they will implement the reconfiguration method developed in this study.

2. Baseline reconfiguration manoeuvres

Of the reconfiguration manoeuvres previously discussed, only the methods used by Lovell *et al.* (2004) and Vaddi *et al.* (2005) offer a simple, impulsive scheme for transferring from ATO $\rightarrow$ ATO, ATO $\rightarrow$ PCO, and PCO $\rightarrow$ PCO formations, as required by the CanX-4&5 mission request for proposal. This method, therefore, will be used in this study as a baseline reconfiguration method for comparison purposes. A brief review of this method is presented here for reference. All three reconfiguration manoeuvres are based upon the HCW equations, a set of linearized equations of relative motion describing the short-term dynamics of the deputy in a local-vertical local-horizontal (LVLH) reference frame centred in the body of the chief. The HCW equations

are given by Clohessy and Wiltshire (1960) as

$$\begin{aligned} \ddot{x} - 2\omega\dot{y} - 3\omega^2 x &= 0 \\ \ddot{y} - 2\omega\dot{x} &= 0 \\ \ddot{z} + \omega^2 z &= 0 \end{aligned} \tag{1}$$

where $\omega = \sqrt{\mu/R^3}$ is the mean orbital rate. These equations are derived under the assumption that the chief is in a circular orbit, that the relative separation between the two spacecraft is negligible compared with the orbital radius, and that no perturbations act on either spacecraft. These assumptions reduce the long-term predictive power of the HCW equations in a real orbital environment. Nevertheless, the equations are still useful: their periodic solutions can be used to develop a set of impulses to transfer a spacecraft between two relative states in the LVLH frame. The set of HCW solutions used to design the baseline reconfiguration manoeuvres by Lovell *et al.* (2004) and Vaddi *et al.* (2005) are

$$\begin{aligned} x &= -\frac{c_1}{2}\cos(\omega t + \beta) + c_4 \\ y &= c_1 \sin(\omega t + \beta) + c_3 - \frac{3}{2}\omega t c_4 \\ z &= c_2 \sin(\omega t + \beta) \end{aligned} \tag{2}$$

where c_i is the coefficient of integration and β is the initial reference trajectory phase angle. Note that c_4 corresponds to the difference between the chief and deputy orbital radii, and must be set to 0 to obtain bounded relative motion. These solutions can also be employed as formation reference trajectories in the LVLH frame. For ATO formations, $c_1 = c_2 = 0$, and $c_3 =$ relative spacecraft separation. For PCO formations, $c_1 = c_2 =$ relative circular orbit radii, and $c_3 = 0$. Using the periodic solutions to the HCW equations given in Equation (2), Lovell *et al.* (2004) derived a set of general impulsive reconfiguration manoeuvres for ATO $\rightarrow$ ATO and ATO $\rightarrow$ PCO manoeuvres. Vaddi *et al.* (2005) used a set of non-singular orbital element differences to develop a two-impulse manoeuvre for the PCO $\rightarrow$ PCO transition. Each impulse is implemented at a specific phase angle β of the relative orbit and in the LVLH direction indicated by the subscript. The equations describing all three baseline manoeuvres are shown in Table 1.

In Table1, c_1 and c_2 are the coefficients of integration from Equation (2), ω is the circular orbital rate, and N is the number of orbits over which the manoeuvre is performed. For the ATO $\rightarrow$ ATO and ATO $\rightarrow$ PCO manoeuvres, $\Delta c_1 = c_{1f} - c_{1i}$, and $\Delta c_2 = c_{2f} - c_{2i}$, where the subscripts i and f denote quantities before and after the manoeuvres respectively. For the PCO $\rightarrow$ PCO manoeuvre, $[\delta a, \delta q1, \delta q2, \delta i, \delta\Omega, \delta\lambda]$ are non-singular orbital element differences, which are derived by Vaddi *et al.* (2005), and $\gamma = \sqrt{a/\mu}$, where a is the semi-major axis of the orbit.

Table 1. Baseline impulsive reconfiguration manoeuvres derived by Lovell *et al.* (2004) and Vaddi *et al.* (2005).

β (rads)	ATO $\rightarrow$ ATO	ATO $\rightarrow$ PCO	PCO $\rightarrow$ PCO
0	$\Delta V_y = -\frac{1}{6N\pi}\omega\Delta c_2$	$\Delta V_y = \frac{1}{16}\omega\Delta c_1 - \frac{1}{6\pi}\omega\Delta c_2$	$\Delta V = \left[-\frac{\sqrt{\delta q_1^2 + \delta q_1^2}}{2\gamma} \quad 0 \quad -\frac{\sqrt{\delta i^2 + \delta\Omega^2 \sin^2 i}}{\gamma}\right]^T$
$\pi/2$	–	$\Delta V_z = -\omega\Delta c_1$	–
π	–	$\Delta V_y = -\frac{1}{8}\omega\Delta c_1$	$\Delta V = \left[\frac{\sqrt{\delta q_1^2 + \delta q_1^2}}{2\gamma} \quad 0 \quad 0\right]^T$
2π	$\Delta V_y = \frac{1}{6N\pi}\omega\Delta c_2$	$\Delta V_y = \frac{1}{16}\omega\Delta c_1 + \frac{1}{6\pi}\omega\Delta c_2$	–

To test the baseline reconfiguration method on the CanX-4&5 mission, a fully nonlinear orbital simulation was developed. A low Earth, sun-synchronous orbit was selected with the orbital elements presented in Table 2. A fourth-order Runge–Kutta integration method with a time step of 0.1 s was used to propagate the nonlinear orbital equations of motion of each satellite, which are given in the geocentric inertial reference (GCI) frame as

$$\ddot{\mathbf{R}}_c = -\frac{\mu \mathbf{R}_c}{R_c^3} + \mathbf{F}(\mathbf{R}_c)_{pert} \tag{3}$$

$$\ddot{\mathbf{R}}_d = -\frac{\mu \mathbf{R}_d}{R_d^3} + \mathbf{F}(\mathbf{R}_d)_{pert} + \mathbf{u}_i \tag{4}$$

where the c and d subscripts refer to the chief and deputy satellites respectively, μ is Earth's gravitational constant, u_i is the control force per unit mass applied to the deputy during formation-flying manoeuvres, and $\mathrm{F(R)}_{pert}$ is the perturbing force acting upon each satellite. In low Earth orbit, the principle perturbing force is the J_2 zonal harmonic of the gravitational field, produced by the oblate shape of the Earth. Higher order terms, from J_3 to J_6, play a smaller role, but were also included in this orbital simulation. The impulses presented in Table 1 are given in the LVLH frame. It is necessary to rotate impulses into the GCI frame before applying them to the orbital equations of motion. The rotation matrix relating the GCI frame to the LVLH frame is

$$\mathbf{C}_{hi}^T(t) = \begin{bmatrix} \dfrac{\mathbf{R}_c}{R_c} & \dfrac{\mathbf{H}_c \times \mathbf{R}_c}{|\mathbf{H}_c \times \mathbf{R}_c|} & \dfrac{\mathbf{H}_c}{H_c} \end{bmatrix} \tag{5}$$

where $\mathbf{H}_c = \mathbf{R}_c \times \dot{\mathbf{R}}_c$ is the chief's angular momentum per unit mass. Once the impulse directions are known in the GCI frame, the impulses are converted into thrusts in order to realistically simulate the reconfiguration manoeuvres. This is accomplished by solving for the thruster on-times, given by

$$T_{on} = \frac{\Delta V}{U_{\max}} \tag{6}$$

where $U_{max} = 0.0008475\,\mathrm{N/kg}$ and is the force per unit mass exerted by the CanX-4&5 thrusters (i.e. a force of 5 mN for a 5.9 kg nanosatellite). The thrusts are then implemented by projecting U_{max} in the direction of the impulses to form u_i, and then integrating Equations (3) and (4) over T_{on}.

The thrusters on CanX-4&5 are sized for low-impulse formation maintenance manoeuvres. Therefore, the deputy must thrust for extended periods of time in order to generate the ΔV values required for each reconfiguration manoeuvre. With the high T_{on} values, the reconfiguration thrusts no longer approximate impulses, which is one of the key assumptions of the baseline method. In addition, these manoeuvres are based on the HCW solutions, which assume a circular orbit with no gravitational perturbations. When the orbital simulation includes eccentricity, J_2–J_6 perturbations and non-impulsive thrusts, the baseline reconfiguration manoeuvres break down and become highly inaccurate.

Table 2. Orbital elements for CanX-4&5 mission.

Eccentricity	0.025
Right ascension	99.56°
Argument of perigee	0°
Altitude at perigee	550 km
Time of perigee passage	0 s
Inclination	97.6°

Table 3. The performance of the baseline reconfiguration method applied to CanX-4&5.

Manoeuvre	ΔV (m/s)	E_x (m)
1,000 m ATO → 500 m ATO	0.0559	74.97
500 m ATO → 50 m PCO	0.1152	37.97
50 m PCO → 100 m PCO	0.06749	14.62

The metrics used to assess each reconfiguration manoeuvre are ΔV, representing the fuel cost, and the position overshoot error[1], defined as

$$E_x = \sqrt{\tilde{x}_1^2 + \tilde{x}_2^2 + \tilde{x}_3^2} = \sqrt{(x - x_T)^2 + (y - y_T)^2 + (z - z_T)^2} \tag{7}$$

where $[x, y, z]$ is the deputy's actual relative position at the end of the reconfiguration manoeuvre and $[x_T, y_T, z_T]$ is the target relative position. Table 3 contains the performance metrics when each baseline reconfiguration manoeuvre from Table 1 is adapted specifically to the CanX-4&5 mission. The high overshoot error values would be unacceptable in an actual formation-flying mission. Clearly, a reconfiguration method that works in a real orbital environment is required.

3. Analytical solution to a state-space model

The analytical solution of the state-space model for the satellites provides an alternate method for calculating the impulses required to reconfigure a satellite formation. The state-space representation of the deputy's relative dynamics with respect to the chief (in the LVLH frame) is given by

$$\dot{\mathbf{x}}(t) = \mathbf{A}\mathbf{x}(t) + \mathbf{B}\mathbf{u} \tag{8}$$

where $\mathbf{x}(t) = [x\ y\ z\ \dot{x}\ \dot{y}\ \dot{z}]^T$, A is the system matrix containing the linearized HCW dynamics, B is the input matrix, and u is the control force (per unit mass) matrix. The deputy's state at any time t is given by the analytical solution of this state-space model

$$\mathbf{x}(t) = e^{\mathbf{A}t}\mathbf{x}(0) + \int_0^t e^{\mathbf{A}(t-\tau)}\mathbf{B}\mathbf{u}(\tau)d\tau \tag{9}$$

Given that the state is a 6×1 column matrix, it is necessary to have two separate three-component impulses to render the problem square and solvable. When the impulses are discretized, the integral in Equation (9) can be replaced by the sum of the two impulses

$$\mathbf{x}(t) = \mathbf{\Phi}(t, 0)\mathbf{x}(0) + \mathbf{B}_1\hat{\mathbf{u}}_1 + \mathbf{B}_2\hat{\mathbf{u}}_2 \tag{10}$$

where $\mathrm{B}_i = \Phi(t, t_i)\mathrm{B}$, t_i is the time at which impulse i is performed, $\hat{\mathbf{u}}_1$ and $\hat{\mathbf{u}}_2$ are the two reconfiguration impulses in the LVLH frame, and $\Phi(t, t_i) = e^{At}$ is the STM for the HCW dynamics. $\Phi(t, t_i)$ must satisfy the following properties:

$$\mathbf{\Phi}(t_i, t_i) = \mathbf{1} \tag{11}$$

$$\dot{\mathbf{\Phi}}(t, t_i) = \mathbf{A}\mathbf{\Phi}(t, t_i) \tag{12}$$

The HCW STM is given analytically by Melton (2000) as

$$\mathbf{\Phi}(t,t_i)=\begin{bmatrix} 4-c & 0 & 0 & s/\omega & 2(1-c)/\omega & 0 \\ 6(s-\omega\Delta t) & 1 & 0 & -2(1-c)/\omega & (4s-3\omega\Delta t)/\omega & 0 \\ 0 & 0 & c & 0 & 0 & s/\omega \\ 3\omega s & 0 & 0 & c & 2s & 0 \\ -6(s-\omega\Delta t) & 0 & 0 & -2s & 4c-3 & 0 \\ 0 & 0 & -\omega s & 0 & 0 & c \end{bmatrix} \tag{13}$$

where $\Delta t = t - t_i$, $s = \sin(\omega t)$ and $c = \cos(\omega t)$. By rearranging Equation (10), and setting the final relative state to the target state, $\mathrm{x}(t) = \mathrm{x}_T(t)$, the two reconfiguration impulses can be determined simultaneously:

$$\begin{bmatrix} \hat{\mathbf{u}}_1 \\ \hat{\mathbf{u}}_2 \end{bmatrix} = [\mathbf{B}_1\ \mathbf{B}_2]^{-1}(\mathbf{x}_T(t) - \mathbf{\Phi}(t,0)\mathbf{x}(0)) \tag{14}$$

Thus, for given impulse times t_1 and t_2, we can solve for the two impulses $\hat{\mathbf{u}}_1$ and $\hat{\mathbf{u}}_2$ required to transfer the deputy from the initial relative state x(0) to the final target state of $\mathrm{x}_T(t)$. These impulses can be applied to the orbital model by first rotating them into the GCI frame, determining their individual T_{on} values from Equation (6), and then solving for the accelerations u_i. Finally, Equations (3) and (4) are integrated over the full reconfiguration time (typically one orbital period) with each thrust applied over the interval $[t_i, t_i + T_{on\_i}]$.

4. State-transition-matrix optimization method

Since the dynamics of the STM are based on the linear HCW equations, the impulses calculated from Equation (14) do not accurately reconfigure the formation when they are applied in a realistic, nonlinear orbital propagator. The principal advantage of the HCW dynamics, however, is that a simple analytical form of the STM exists, allowing calculations to be carried out with a minimum amount of computational effort. CanX-4&5 satellites will be equipped with on-board computers dedicated to running a formation-flying control algorithm. Each computer will feature a 7 MHz ARM7 microcontroller with 2 MB of SRAM and 256 MB of flash memory. As a result of the very limited processing power of these computers, the formation-flying control algorithm—including the formation reconfiguration code—must be computationally efficient, even at the expense of performance accuracy.

The inaccuracies of the HCW STM can be circumvented by posing the reconfiguration impulse design as an optimization problem. In Equation (14), t_i, the time at which each impulse is performed during the reconfiguration orbit, is an independent variable that can strongly affect the accuracy of the manoeuvres. By optimizing the t_i value for each impulse and determining its effects on the reconfiguration accuracy using a high-fidelity orbital propagator, it is possible to design reconfiguration manoeuvres which are accurate, have moderate ΔV requirements, and work in a realistic, nonlinear orbital simulator.

The STM optimization problem can be posed as:

$$\text{Minimize}: \quad \Delta V_{total} = \sum_{i=1}^{2} \Delta V_i, \quad \text{where } \Delta V_i = U_{max} T_{on\_i}$$

$$\begin{aligned} \text{With respect to :} \quad & t_1 \text{ and } t_2 \\ \text{Subject to :} \quad & |\tilde{x}_i| \leq 2.5, \text{ for } i = 1, 2, 3 \\ & |\tilde{v}_i| \leq 0.1, \text{ for } i = 1, 2, 3 \\ & 0 \leq t_1 < t_2 < T_{period} \end{aligned}$$

where T_{on_i} is the individual thruster on times, t_1 and t_2 the start time for each impulse, and $\tilde{x}_i$ and $\tilde{v}_i$ are the position and velocity overshoot errors in each coordinate direction of the LVLH frame, as defined in Equation (7). After a full exploration of the design space (see Sections 4 and 5), constraints of 2.5m on the position overshoot error and of 0.1 m/s on the velocity overshoot error were selected for the CanX-4&5 mission. The constraints on the impulse times simply indicate that the first impulse should not occur prior to beginning the reconfiguration orbit, that the first impulse should precede the second, and that the second impulse must occur before the end of the reconfiguration orbit. ΔV_{total} was selected as the objective function even though the main impetus for the new reconfiguration scheme is to minimize the overshoot errors associated with the manoeuvre. The reasons for this are twofold. First, ΔV_{total} represents the fuel requirements of each reconfiguration manoeuvre, and minimizing this value is desirable. Second, the overshoot errors have six components, whereas the ΔV_{total} has only one, which simplifies the optimization process. Therefore, ΔV_{total} is minimized with tight constraints applied to the overshoot errors such that, when a feasible solution is found, the manoeuvre will have an acceptable accuracy for a minimum ΔV.

It would be technically possible to structure the reconfiguration optimization around the fully perturbed, nonlinear equations of orbital motion and forgo the STM altogether. Such an optimization problem, however, would require eight design variables (the three Cartesian impulse directions plus the t_i value for each of the two impulses), increasing the complexity of optimization procedure significantly. By including the STM, the six impulse directions are solved for us, simplifying the optimization problem to two design variables. And although these impulse directions are initially inaccurate because of the linear HCW dynamics, the optimizer adjusts the t_i values to compensate and achieve accurate solutions.

The STM optimization algorithm is outlined in Figure 1. The main point of this algorithm is that, although the impulses are computed using the linear dynamics of the HCW equations, they are optimized using the full, nonlinear orbital equations of motion with J_2 to J_6 perturbations and implemented non-impulsively. The final impulse solutions would not be accurate in a simple, linearized orbital simulation, but they have been optimized to function correctly in a realistic, nonlinear environment.

In Figure 1, $\mathbf{x}(t) = [x\ y\ z\ \dot{x}\ \dot{y}\ \dot{z}]^T$ in the LVLH frame and $\mathbf{X}(t) = [\mathbf{R}_c\ \dot{\mathbf{R}}_c\ \mathbf{R}_d\ \dot{\mathbf{R}}_d]^T$ in the GCI frame, where $\mathbf{R}_c = [XYZ]^T$, etc.

Since the optimization problem is highly constrained, Sequential Quadratic Programming (SQP) was selected to optimize the ΔV_{total} value for each reconfiguration manoeuvre. SQP is a robust optimization algorithm which models the function at the current point as a quadratic approximation and then uses the minimum of that model to find the next point. During each optimization step, a Hessian matrix is assembled from the second-order partial derivatives of the function and is used in combination with a Jacobian of the constraints to determine the optimization search direction, p. A step length in the direction of p is found from a simple back-tracking line search that tests for a sufficient decrease of $\phi(t_1, t_2, \mu)$, a penalized objective function defined as

$$\varphi(t_1, t_2, \mu) = f(t_1, t_2) + \frac{1}{\mu}\|\nabla c\| \tag{15}$$

where μ is a positive penalty parameter and $\|\nabla c\|$ is the L1 norm of the constraints.

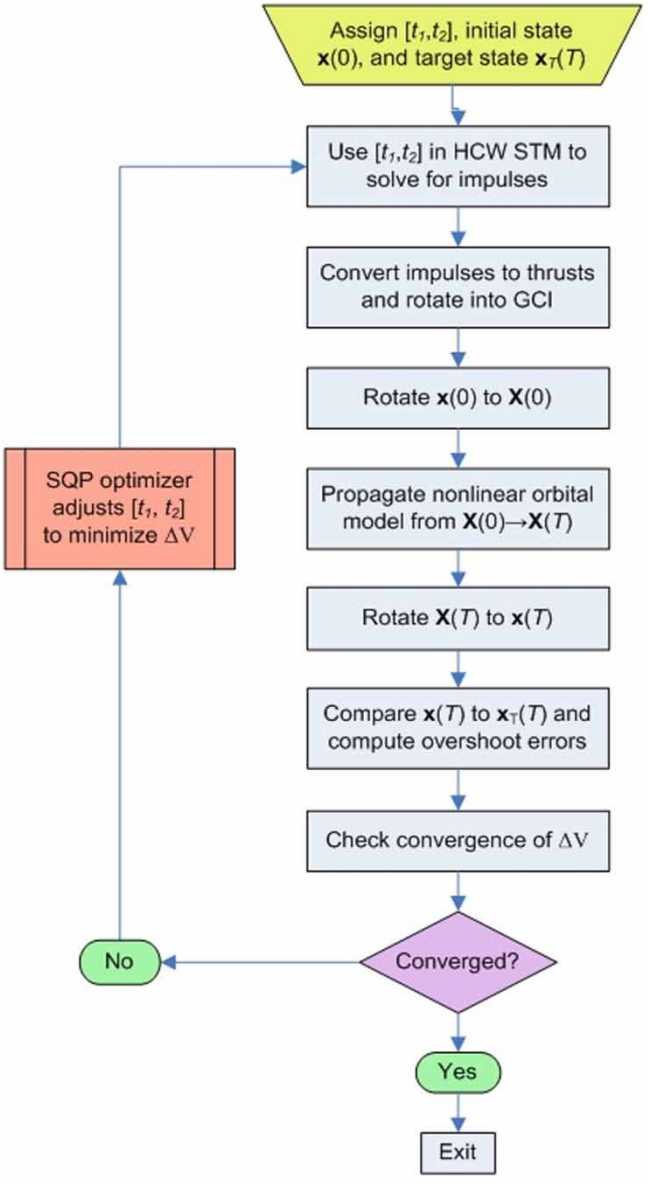

Figure 1. The state-transition-matrix optimization algorithm.

5. Design-space exploration

The formation-flying reconfiguration optimization problem consists of two design variables and a single objective function subject to multiple constraints, making it possible to completely explore the design space for each manoeuvre. This is useful for identifying feasible regions to select as the starting points for the STM optimization procedure described in Figure 1. Figure 2 illustrates the design-space surface for the 1,000 m ATO $\rightarrow$ 500 m ATO manoeuvre. The prominent ridge dominating the centre of the design space is an artefact caused by the STM: when the two impulse start times are equal, the matrix $[B_1\ B_2]^{-1}$ in Equation (14) is singular. As a result,

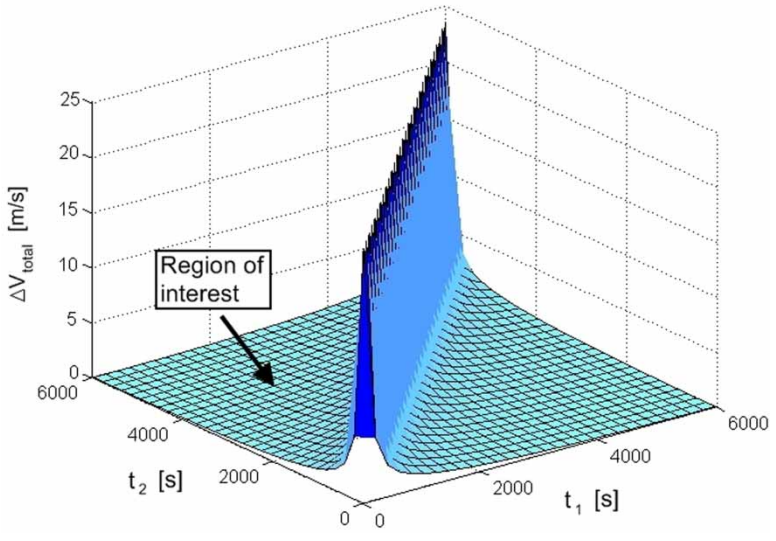

Figure 2. The design space for the ATO → ATO reconfiguration manoeuvre optimization.

the impulses $\hat{\mathbf{u}}_1$ and $\hat{\mathbf{u}}_2$ are divergent. In addition, $t_1 > t_2$ on the right side of the ridge. Since this violates one of the optimization constraints, this region is unfeasible and is ignored.

In the absence of constraints, the region of interest in Figure 2 is unimodal and smooth. Figure 3 illustrates the constrained design space, where a contour plot of the objective function is shown with the contours of the constraints, c_i, overlaid at $c_i = 0$ (for $i = 1, 2 \ldots 9$).

The active constraints are the $\tilde{x}_1$ and $\tilde{x}_2$ overshoot errors. The intersection between these two constraints form small, isolated feasible regions. The constrained design space is multimodal, presenting difficulties for the optimization algorithm. As a gradient-based optimizer, SQP performs best when the starting point lies in a feasible region. In this study, the need for tight constraints on the overshoot errors has reduced the size of the feasible regions to the point where random starting locations will mostly be unfeasible. A domain-spanning optimization method, such as a genetic algorithm with penalty functions to approximate the constraints, would be applicable but could easily miss the small global minimum and would not be as precise as the SQP method. Instead, by using Figure 3 to identify the local minima, it is possible to select a starting point for the SQP method in each of the feasible regions and allow the optimizer to precisely locate the global minima. It is worth noting that ΔV_{total} and E_x are competing metrics: tightening the constraints to reduce E_x will shrink the feasible regions in Figure 3, and the current global minimum will be quickly eliminated. The next local minima to the right will take its place as the global minimum, but with a higher ΔV_{total} value than the original. This performance trade-off is analysed in Section 5.

Figure 4 shows a contour plot of the constrained design space for the ATO → PCO manoeuvre. Like the contour plot for the ATO → ATO manoeuvre, the feasible regions are small, isolated areas defined by the $\tilde{x}_1$ and $\tilde{x}_2$ overshoot error constraints. Since the series of feasible regions runs parallel to the contours of the objective function, tightening the constraints will simultaneously reduce the size of all feasible regions. The secondary ridge which dominates the centre of Figure 4 is caused by the stronger impulses necessary to implement the plane change near the perigee during the ATO → PCO manoeuvre.

Figure 5 shows the contour plot of the constrained design space for the PCO → PCO manoeuvre. The feasible region is much larger than the previous manoeuvres with an easily identifiable

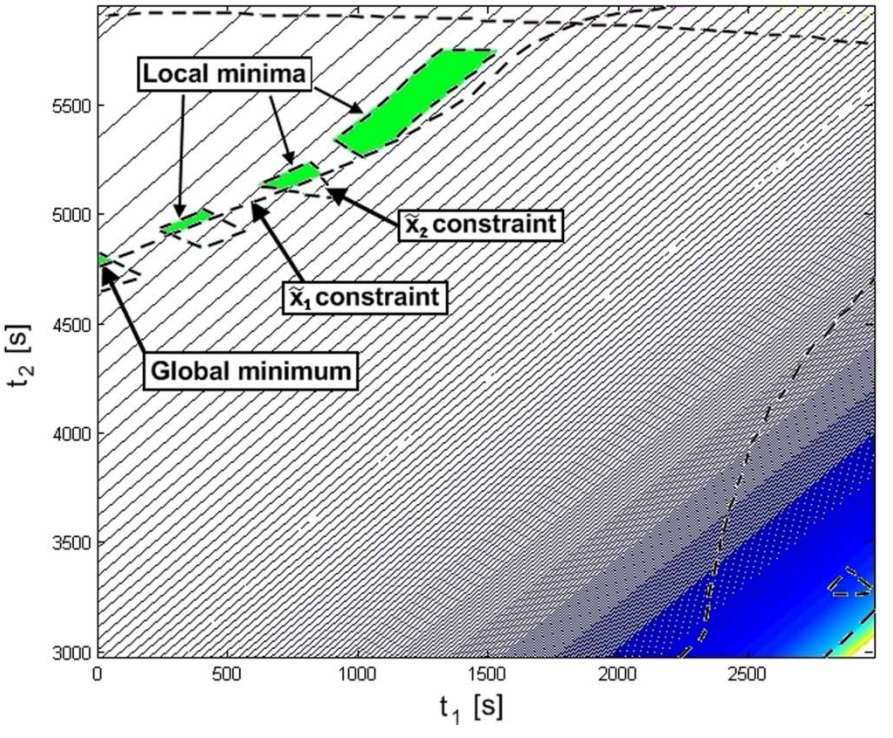

Figure 3. Contour plot for the ATO → ATO manoeuvre optimization.

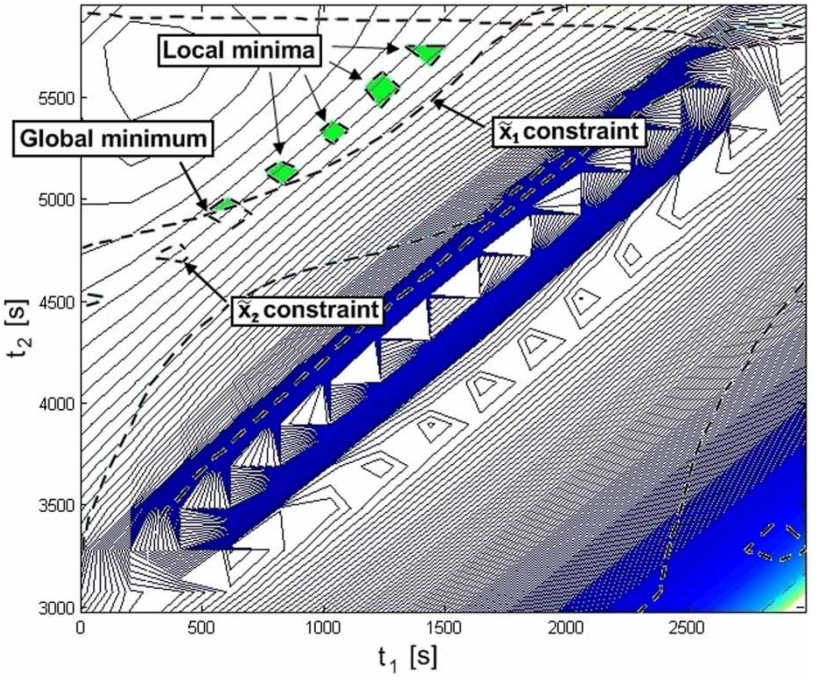

Figure 4. Contour plot for the ATO → PCO manoeuvre optimization.

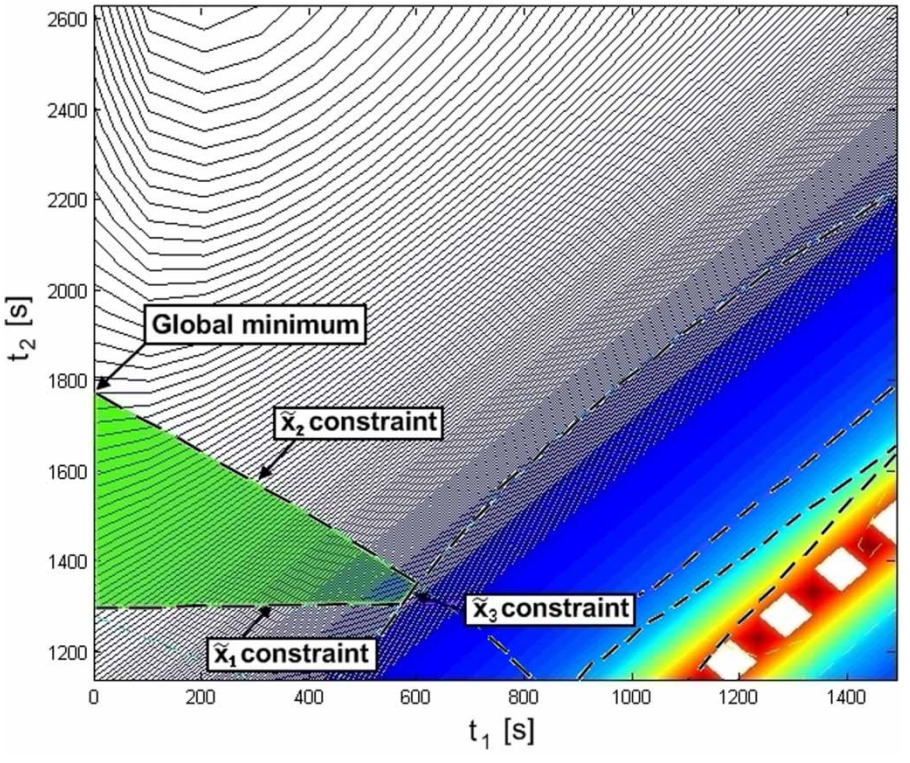

Figure 5. Contour plot for the PCO → PCO manoeuvre optimization.

global minimum and no local minima. At the global minimum, the active constraints are $t_1 \geq 0$ and $\tilde{x}_2 \leq 2.5\,\text{m}$. There is a direct trade off between the $\tilde{x}_2$ constraint and the ΔV_{total} objective function: relaxing $\tilde{x}_2$ will decrease the ΔV_{total} values but increase the overshoot errors, and vice versa.

6. Performance trade-off

As previously mentioned, the ΔV_{total} requirements and overshoot errors are competing metrics in the reconfiguration optimization procedure. The direct relationship between these metrics can be assessed for each manoeuvre by alternately tightening and relaxing the overshoot error constraints and determining the impact on the ΔV_{total} value of the optimized solution. This will establish a Pareto frontier of potential reconfiguration designs based on different weighting choices for each metric. This enables us to select a design which strikes an appropriate balance between fuel requirements and overshoot errors while avoiding Pareto inefficient design choices that do not lie on the frontier.

Figure 6 shows the Pareto frontier for the ATO → ATO manoeuvre. The baseline reconfiguration manoeuvre is also indicated on this graph, and since it lies far inside the Pareto frontier, it is not Pareto efficient and therefore not a viable reconfiguration design option. Any of the designs lying along the frontier would offer superior performance, but since more emphasis is placed on manoeuvre accuracy in this study, a design on the upper left section of the frontier has been selected as the final solution.

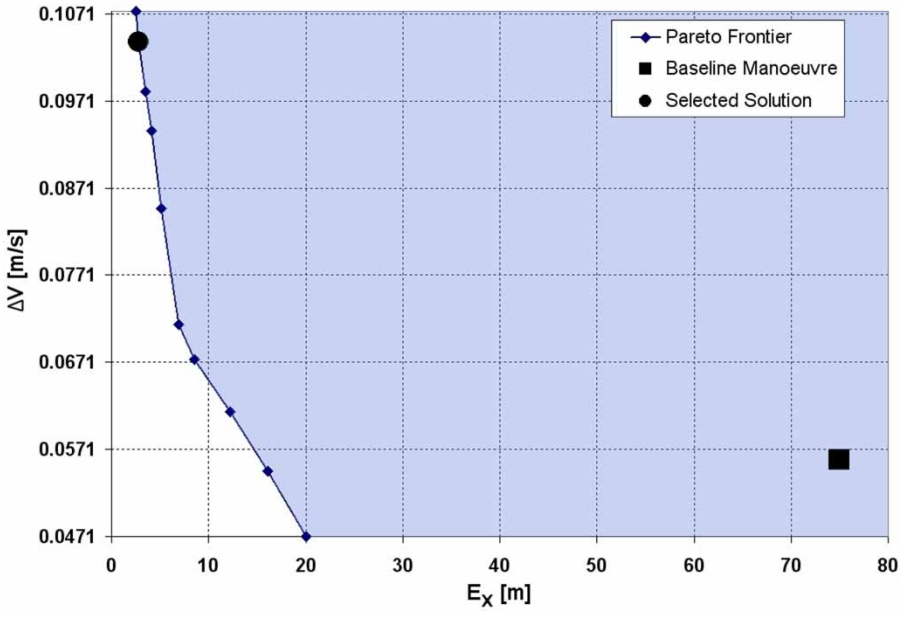

Figure 6. Pareto frontier for the ATO → ATO manoeuvre design.

Figures 7 and 8 show the Pareto frontiers for the ATO → PCO and PCO → PCO reconfiguration manoeuvres. In each case, the baseline manoeuvres are also identified and are clearly not Pareto efficient. The selected reconfiguration solution is represented by a circle in each case.

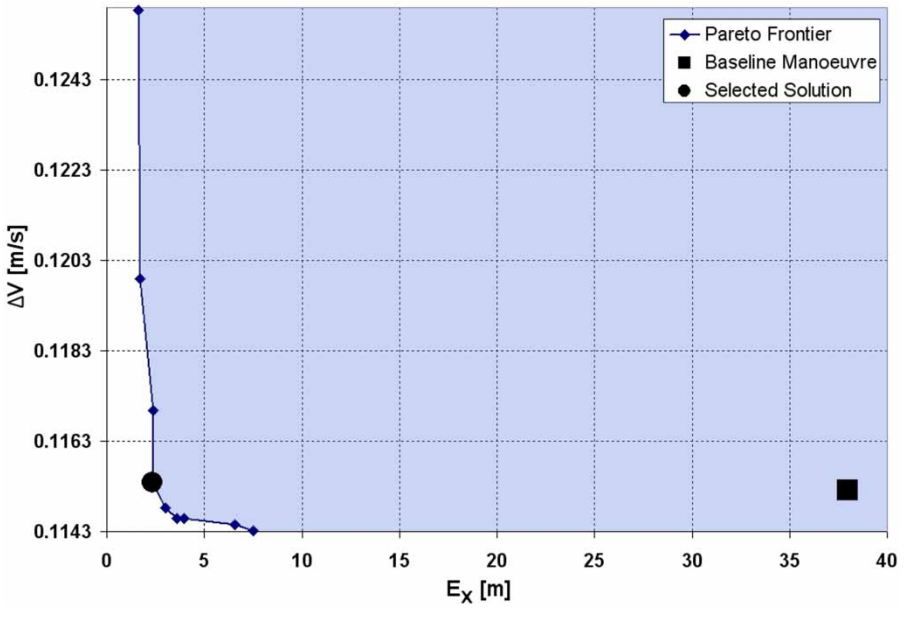

Figure 7. Pareto frontier for the ATO → PCO manoeuvre design.

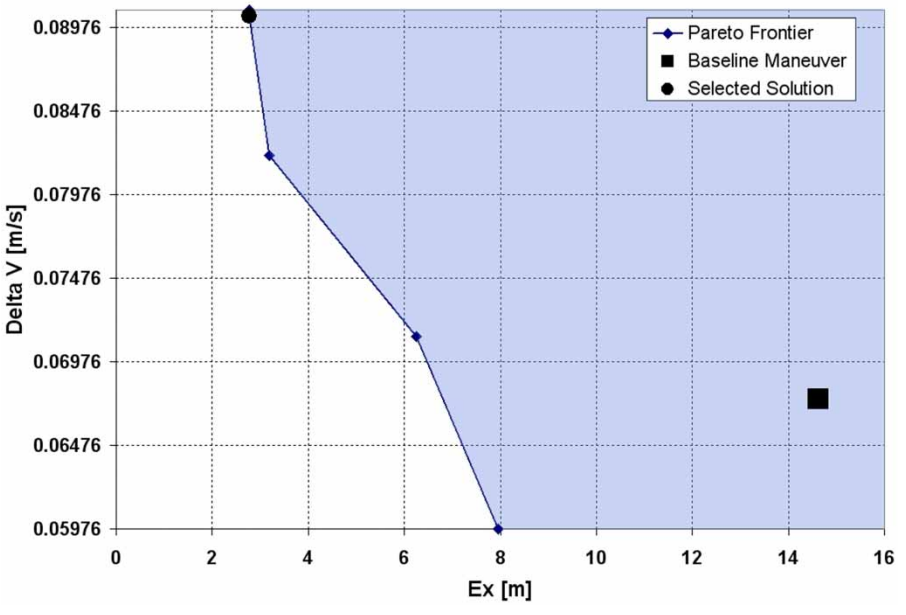

Figure 8. Pareto frontier for the PCO → PCO manoeuvre design.

It should be noted that is it not possible to extend the Pareto frontiers to zero overshoot error, since the feasible regions in Figures 3–5 disappear as $E_x \rightarrow 0$. This inability to achieve perfect accuracy is due to the inherent limitations of the linear HCW STM.

7. Reconfiguration optimization results

The feasible region containing the global minimum was identified in the design space of each reconfiguration manoeuvre. A starting point $[t_1, t_2]$ was selected from the feasible region and the optimizer was run. In each case, the orbital simulator propagated the nonlinear orbital equations of motion (Equations [3] and [4]) with J_2–J_6 perturbations using a fourth-order Runge–Kutta method with a time step of 0.1 s. All thrusts were implemented non-impulsively with the thrust level set to 5 mN, as determined by the CanX-4&5 propulsion system. The orbital elements used for each simulation are given in Table 1.

Since the optimization problem was well posed and the objective function unimodal within the feasible region(s), the SQP optimization algorithm was able to readily converge to the constrained global minimum for each manoeuvre. Figure 9 depicts the convergence of the SQP algorithm for the ATO → ATO manoeuvre from three separate starting points in the feasible region. In each case, the algorithm converges within 6–13 iterations. Similarly, the ATO → PCO and PCO → PCO manoeuvres converge to their respective global minima within approximately 15 iterations when the starting points lie within the appropriate feasible regions. Note that the large dips in Figure 9 below the convergence level occur when the optimizer steps outside of the feasible region.

Once the optimization algorithm had located the global minimum for each manoeuvre, the resulting impulse start times and corresponding T_{on} values were used to test the reconfiguration trajectory solutions in a fully nonlinear simulation (including J_2–J_6 perturbations). Figures 10–12 show the STM optimized reconfiguration trajectory solutions projected onto the xy-plane and yz-plane of the LVLH reference frame. The small cross represents the initial relative position of

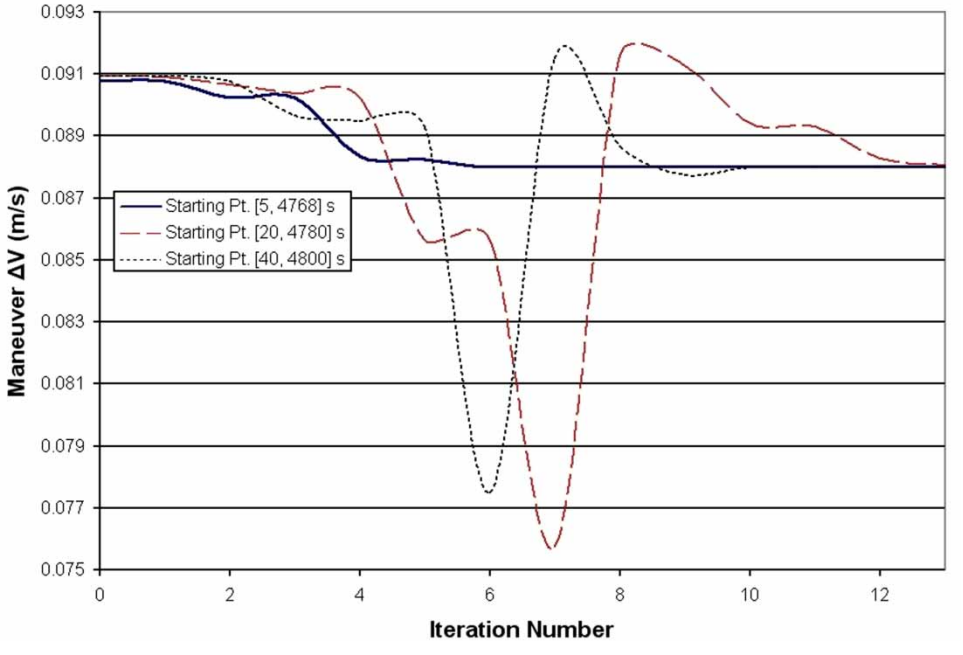

Figure 9. Convergence of the ATO → ATO manoeuvre optimization.

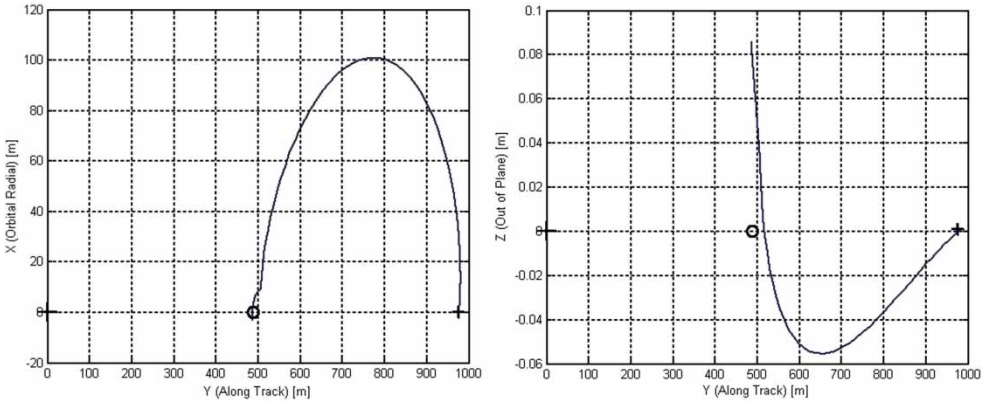

Figure 10. The 1,000 m ATO → 500 m ATO reconfiguration manoeuvre.

the deputy, the circle identifies the target state, and the large cross represents the location of the chief.

Table 4 contains the performance metrics of each STM optimized reconfiguration manoeuvre. As anticipated, the SQP optimizer located the global minimum on the overshoot constraints for each manoeuvre. As a result, the accuracy of the manoeuvres has been significantly improved over the baseline for marginal increases in the ΔV requirements. The thrust start times assume that the reconfiguration manoeuvres begin at $t = 0$ sec and end one period later at $t = T = 5955$ sec for the ATO → ATO and ATO → PCO, and end at $t = T/2$ for the PCO → PCO manoeuvre.

Table 5 gives the change in each metric between the baseline and STM optimized method. In each case, the STM optimized trajectories reach the target positions with a much greater accuracy than the equivalent baseline trajectories. But this improved accuracy comes at the cost of

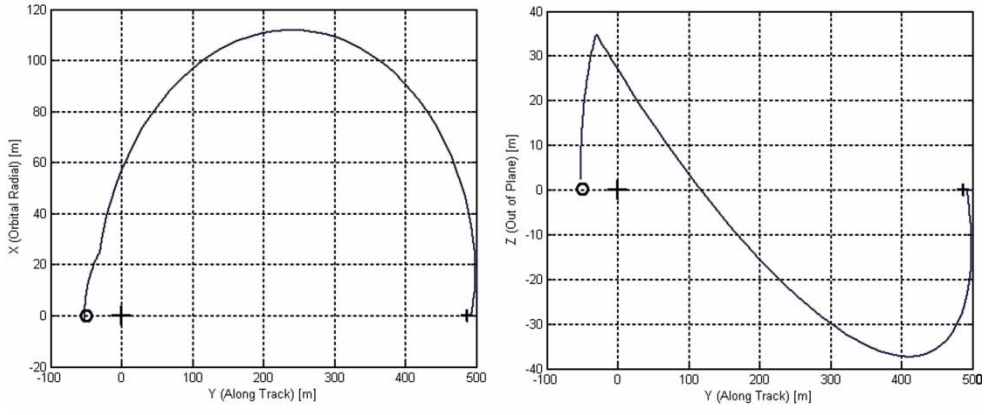

Figure 11. The 500 m ATO → 50 m PCO reconfiguration manoeuvre.

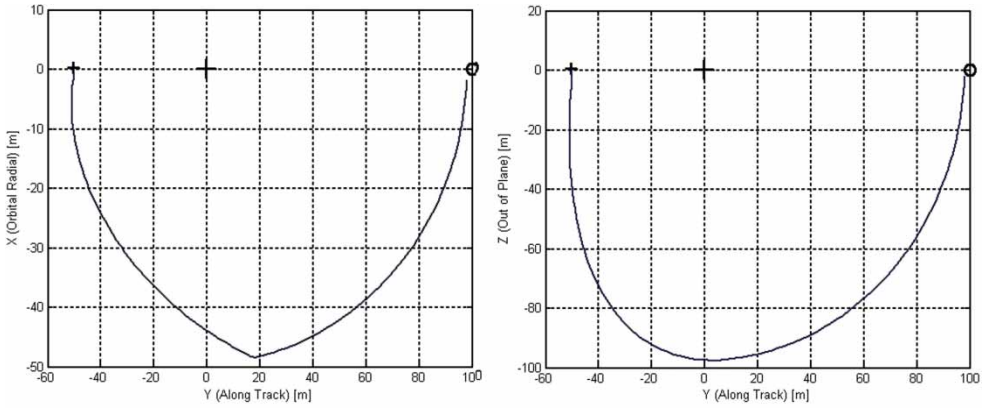

Figure 12. The 50 m PCO → 100 m PCO reconfiguration manoeuvre.

Table 4. The performance of the state transition matrix optimization method applied to CanX-4&5.

Manoeuvre	Impulse direction (LVLH)	$[t_1, t_2]$ (s)	$[T_{on-1}, T_{on-2}]$ (s)	ΔV (m/s)	E_x (m)
1,000 m ATO → 500 m ATO	$\begin{bmatrix}0.8176\\0.5758\\0\end{bmatrix}, \begin{bmatrix}0.8267\\-0.5626\\0\end{bmatrix}$	[4.35, 4768.73]	[51.57, 51.54]	0.0880	2.713
500 m ATO → 50 m PCO	$\begin{bmatrix}0.6574\\0.4199\\-0.6258\end{bmatrix}, \begin{bmatrix}0.6259\\-0.4107\\-0.6631\end{bmatrix}$	[854.15, 5183.20]	[73.47, 74.31]	0.1204	3.297
50 m PCO → 100 m PCO	$\begin{bmatrix}0.05133\\-0.2309\\-0.9716\end{bmatrix}, \begin{bmatrix}0.9210\\0.3891\\0.01863\end{bmatrix}$	[0.57, 1639.69]	[63.93, 37.69]	0.0849	3.491

increased ΔV requirements. CanX-4&5 are allocated approximately 300 mL of liquefied sulphur-hexafluoride (SF_6) as a propellant. With an I_{SP} of 35 s, this provides a total $\Delta V = 14.22$ m/s. Table 5 gives the percentage of the total ΔV being used by the STM optimized reconfiguration manoeuvres. In total, the STM optimized manoeuvres account for 2.063% of the available ΔV,

Table 5. The change in performance metrics between the baseline and STM optimized manoeuvres.

Manoeuvre	Change in ΔV (m/s)	% of total ΔV	Change in E_x (m)
1,000 m ATO → 500 m ATO	+0.0321	0.6188	−71.29
500 m ATO → 50 m PCO	+0.0052	0.8467	−34.67
50 m PCO → 100 m PCO	+0.0174	0.5970	−11.13

whereas the baseline manoeuvres would account for only 1.678%. This amounts to a 0.385% increase in ΔV required by the new reconfiguration manoeuvres, which is deemed an acceptable cost for such a significant improvement in manoeuvre accuracy.

8. Thrust timing error analysis

In the simulated orbital environment developed for this study, it is possible to implement the STM optimized reconfiguration impulses at precisely the right time to achieve highly accurate manoeuvres. On orbit, however, higher order gravitational harmonics and atmospheric drag will perturb the formation to a greater extent than predicted by our orbital propagator. After performing 50 orbits in each formation, it is conceivable that these perturbations will introduce some phase lead or lag into the relative orbits. In reality, therefore, the deputy might not have the same relative state as that predicted by the simulator, and the reconfiguration impulses would be implemented at the wrong times. Although these timing errors could be minimized by increasing the fidelity of the orbital simulator, it is instructive to determine the robustness of each reconfiguration solution found in this study using just J_2–J_6 perturbations.

To this end, timing errors were introduced systematically to all three manoeuvres: the start time of each impulse was varied between −10 sec and +10 sec from its optimal value, and the E_x values were recorded. The resulting increases in the overshoot error are shown in Table 6. The bold values represent the overshoot errors when one impulse start time, either t_1 or t_2, is held constant while the other is varied. The centre value of each 3×3 grid indicates the optimized value, where $\Delta t_1 = \Delta t_2 = 0$. A few general trends can be observed in Table 6. For the ATO → ATO and ATO → PCO manoeuvres, the $\Delta t_2 = 0$ column of each 3×3 grid indicates that the accuracy of the reconfiguration is relatively insensitive to timing errors on the first impulse. Values in the $\Delta t_1 = 0$ row show that the manoeuvres are highly sensitive to errors on the second impulse, however. For the PCO → PCO manoeuvre, the accuracy is least affected by changes in the diagonal where both thrusts are either too early or too late. For all other timing combinations, however, the overshoot errors increase substantially.

Table 6. Thrust timing error analysis.

		E_x (m)		
Manoeuvre	Δt_2 Δt_1	−10 sec	0 sec	+10 sec
1,000 m ATO → 500 m ATO	−10 sec	68.2	6.9	58.0
	0 sec	60.2	2.71	61.3
	+10 sec	55.3	8.6	64.6
500 m ATO → 50 m PCO	−10 sec	71.1	10.1	76.6
	0 sec	70.6	3.29	75.7
	+10 sec	68.9	10.3	74.8
50 m PCO → 100m PCO	−10 sec	5.7	15.1	30.6
	0 sec	15.0	3.49	18.9
	+10 sec	34.2	17.6	9.8

9. Conclusions

Using an STM based on the linear HCW equations and an SQP optimization algorithm acting on a realistic, fully non-linear orbital simulation, a new method for calculating optimal reconfiguration thrusts for formation-flying satellites was presented. This STM optimization technique was applied to the CanX-4&5 mission plan, which calls for reconfiguration manoeuvres between along track orbit formations and projected circular orbit formations. In each case, the method greatly improved the accuracy of the reconfiguration manoeuvres over the baseline reconfiguration strategy for a marginal increase in the ΔV requirements. Furthermore, the method is relatively robust to timing errors on the first thrust in the sequence, and is simple to implement from an engineering standpoint.

Note

1. A similar equation can be written for the velocity overshoot error, $E_v = \sqrt{(v_x - v_{xT})^2 + (v_y - v_{yT})^2 + (v_z - v_{zT})^2}$. However, the velocity errors associated with the reconfiguration manoeuvres in this study are comparatively low and as such E_v is not considered a primary performance metric. The velocity errors are still considered as optimization constraints in Section 3.

Acknowledgements

The authors would like to gratefully acknowledge the ongoing contributions of the CanX student team: Norman Deschamps, Jonathan Gryzmisch, Liam O'Brian, Nathan Orr, Adam Philip, Chris Short and Maria Short. In addition, the authors wish to thank the SFL staff for their support: Alex Beattie, Stuart Eagleson, Cordell Grant, Daniel Kekez, Stephen Mauthe, Freddy Pranajaya, Tarun Tuli, and Rob Zee.

References

Boutonnet, A., and Martinot, V. 2005. Optimal invariant spacecraft formation deployment with collision risk management. *Journal of Spacecraft and Rockets*, 42 (5), 913–920.

Clohessy, W., and Wiltshire, R. 1960. Terminal guidance system for satellite rendezvous. *Journal of the Aerospace Sciences*, 27 (9), 653–658.

Dimitriu, D., Marques, S., Lima, P., Bastante, J., Araujo, J., Penin, L., Caramagno, A., and Udrea, B. 2007. Optimal guidance and decentralized state estimation applied to a formation-flying demonstration mission in GTO. *Control Theory and Applications, IET*, 1 (2), 532–544.

Gim, D., and Alfriend, K. 2003. State transition matrix of relative motion for the perturbed noncircular reference orbit. *Journal of Guidance, Control, and Dynamics*, 26 (6), 956–971.

Lee, D., Cochran, J.E., and Jo, J.H. 2007. Solutions to the variational equations for relative motion of satellites. *Journal of Guidance, Control, and Dynamics*, 30 (3), 669–678.

Lovell, T., and Tragesser, S. 2004. Near-optimal reconfiguration and maintenance of close spacecraft formations. *Annals of the New York Academy of Sciences*, 1017: 158–176.

Mailhe, L., and Guzman, J. 2004. Initialization and resizing of formation-flying using global and local optimization methods. *In*: *Proceedings of the IEEE Aerospace Conference*. Piscataway, NJ: IEEE, 556.

Melton, R. 2000. Time-explicit representation of relative motion between elliptical orbits. *Journal of Guidance, Control, and Dynamics*, 23 (4), 604–610.

Vaddi, S., Alfriend, K., Vadali, S., and Sengupta, P. 2005. Formation establishment and reconfiguration using impulsive control. *Journal of Guidance, Control, and Dynamics*, 28 (2), 262–268.

Yamanaka, K., and Ankersen, F. 2002. New state transition matrix for relative motion on an arbitrary elliptical orbit. *Journal of Guidance, Control, and Dynamics*, 25 (1), 60–66.

Yan, H., and Alfriend, K. 2007. Approximate minimum energy control laws for low-thrust formation reconfiguration. *Journal of Guidance, Control, and Dynamics*, 30 (4), 1182–1186.